JOURNAL OF GEOPHYSICAL RESEARCH: OCEANS, VOL. 118, 2623–2639, doi:10.1002/jgrc.20189, 2013

Role of asymmetric tidal mixing in the subtidal dynamics of narrow estuaries

Peng Cheng,[1,2] Huib E. de Swart,[3] and Arnoldo Valle-Levinson[4]

Received 25 June 2012; revised 26 March 2013; accepted 1 April 2013; published 29 May 2013.

[1] The role of asymmetric tidal mixing (ATM) in subtidal estuarine dynamics is investigated using a series of generic numerical experiments that simulate narrow estuaries under different stratification and external forcing conditions. The focus is on quantifying the characteristics of ATM-induced flow and its contributions to stratification and salt transport. The flow induced by ATM has a two-layer vertical structure in periodically stratified estuaries, similar to that of the density-driven flow. It has a three-layer vertical structure in the central regime of weakly stratified estuaries, and a reverse two-layer structure in highly stratified estuaries. The changes in vertical distribution of ATM-induced flows result from the influence of stratification on the covariance of eddy viscosity and vertical shear. Such covariance represents the driving force of ATM-induced flow in the tidally averaged momentum equation. Compared to density-driven flow, ATM-induced flow dominates in periodically stratified estuaries with strong tides, has the same order of magnitude in weakly stratified estuaries with moderate tides, and is less important in highly stratified estuaries with weak tides. In contrast to density-driven flow that always increases estuarine stratification and transports salt landward, the ATM-induced flow exhibits different behaviors because of its varying vertical structure. In estuaries with strong tides, ATM-induced flow tends to enhance stratification and to transport salt landward, similar to density-driven flow. In estuaries with weak tides, ATM-induced flow tends to reduce stratification and to transport salt seaward.

Citation: Cheng, P., H. E. de Swart, and A. Valle-Levinson (2013), Role of asymmetric tidal mixing in the subtidal dynamics of narrow estuaries, *J. Geophys. Res. Oceans*, *118*, 2623–2639, doi:10.1002/jgrc.20189.

1. Introduction

[2] The horizontal salinity gradient has long been recognized as the dominant mechanism driving residual flow in estuaries [*Pritchard*, 1956]. The dynamics of estuarine circulation is assumed to be determined by a linear momentum balance between horizontal pressure gradient and vertical shear stress divergence that is parameterized with a constant eddy viscosity, while tidal influences on advection and turbulent mixing are neglected [*Hansen and Rattray*, 1965; *Chatwin*, 1976]. As a major external forcing, tides can contribute to the creation of subtidal estuarine currents through nonlinearities in advection terms [*Ianniello*, 1977; *Li and O'Donnell*, 2005; *Winant*, 2008], interaction with bottom bathymetry [*Zimmerman*, 1980], as well as internal tidal asymmetry that was first introduced by *Jay* [1991]. Because stratification tends to increase the vertical shear of currents, tidal velocity profiles become asymmetric during a tidal cycle. Customarily, more sheared flows appear on ebb than on flood, resulting in a "net" flow that has a two-layer structure similar to that of the gravitational circulation [*Jay*, 1991; *Stacey et al*., 2001]. The conceptual analysis of the residual flow induced by the flood-ebb asymmetry in stratification (or turbulent mixing) has indicated that the covariance between eddy viscosity and vertical shear acts as an important driving force for estuarine circulation and needs to be included in the linear momentum balance.

[3] Using observational data in the Hudson River, *Geyer et al*. [2000] calculated tidal and tidally averaged shear stresses, and demonstrated that the vertical structure of the tidally averaged stress mainly results from tidal variations. Subsequent studies separated the tidally averaged divergence of shear stress into two components: the tidal mean and the tidal fluctuation that represented the contribution of asymmetric tidal mixing (ATM) in the tidally averaged momentum equation. With this treatment of the shear stress

[1]Horn Point Laboratory, University of Maryland Center for Environmental Science, Cambridge, Maryland, USA.
[2]College of Ocean and Earth Sciences, Xiamen University, Xiamen, China.
[3]Institute for Marine and Atmospheric Research Utrecht, Utrecht University, Utrecht, Netherlands.
[4]Department of Civil and Coastal Engineering, University of Florida, Gainesville, Florida, USA.

Corresponding author: P. Cheng, Horn Point Laboratory, University of Maryland Center for Environmental Science, Cambridge, MD 21613, USA. (pcheng@umces.edu)

2169-9275/13/10.1002/jgrc.20189

divergence, the residual flow induced by ATM can be explicitly obtained by solving the momentum equation using analytical [*Cheng et al*., 2010] and numerical [*Burchard and Hetland*, 2010; *Burchard et al*., 2011; *Cheng et al*., 2011] models. Those studies confirmed that typical ATM, i.e., stronger mixing during flood than ebb tides, can produce a two-layer residual flow with a vertical structure that is similar to that of the gravitational circulation. They further revealed that in periodically stratified estuaries the residual flow generated by ATM is larger than that driven by longitudinal density gradients.

[4] The mechanism of ATM is highly sensitive to tidal forcing and might exhibit various characteristics under different stratification conditions, leading to marked contrasts in estuarine circulation patterns and mixing processes. Previous studies have provided evidence of ATM-induced flows in estuaries with particularly strong tides such as the Columbia River estuary [*Jay*, 1991] and in idealized numerical model settings [*Burchard and Hetland*, 2010; *Cheng et al*., 2011]. However, little is known about the importance of ATM in different types of estuaries. *Cheng et al*. [2011] examined three types of estuaries: periodically stratified, weakly stratified, and highly stratified, each with an idealized numerical experiment. Their numerical model was specified with strong tides and gave insufficient details for different types of estuaries because of the limited number of experiments. The latter study provided the main motivation for the present investigation, i.e., to conduct experiments for a much wider range of stratification and tidal forcing conditions than in previous efforts. Results are mapped into a parameter space in order to separate the influence of different stratification and tidal forcing conditions, and thereby distinct estuarine types. The main purpose of this study is to provide a general understanding of the role of ATM in sutbidal estuarine dynamics. Specific objectives include delineating the vertical pattern and the strength of ATM-induced residual flow. Moreover, in analogy to the classic studies of estuarine circulation by *Pritchard* [1956] and *Hansen and Rattray* [1965], the relative importance of ATM-induced flow with respect to that of density-driven flow in producing stratification and salt fluxes is assessed.

[5] This study is restricted to narrow estuaries in which the influence of lateral processes and Coriolis acceleration on along-estuary flow is weak. In narrow estuaries, the tidal variability of tidal current structure results mainly from ATM through the straining of the density field [*Simpson et al*., 1990; *Jay*, 1991], while in wide estuaries with transverse varying bathymetry, tidal variability might be largely caused by lateral processes [*Burchard and Schuttelaars*, 2012]. Therefore, the choice of narrow estuaries is convenient to isolate and highlight the role of ATM. Spring-neap variability of tides, which is important in realistic estuaries, has been neglected in order to provide general tidal conditions. But such variability may be diagnostically drawn form results with different tidal forcing prescriptions.

[6] The remainder of this paper is structured as follows: In section 2, the numerical model configuration and the methods to decompose residual currents and to calculate salt transport are presented. In section 3, numerical experiments are undertaken to examine the characteristics of ATM-induced flow in different types of estuaries. In particular, the vertical pattern, the strength, the importance relative to gravitational circulation, and the contributions to stratification and salt balance are analyzed. In section 4, the discussion concentrates on the driving mechanisms of ATM, the scaling of ATM-induced flows, and a classification of estuaries in view of tidal mixing. Section 5 summarizes the main findings of the study.

2. Methods

2.1. Numerical Model

[7] A series of generic numerical experiments were carried out using the Regional Ocean Modeling System, which is a free-surface, hydrostatic, primitive equations ocean model that uses stretched, terrain-following vertical coordinates, and orthogonal curvilinear horizontal coordinates on an Arakawa C-grid [*Haidvogel et al*., 2000; *Shchepetkin and McWilliams*, 2005]. The model domain is designed as an estuary-shelf system (Figure 1). The part of the domain corresponding to the estuary is straight, 500 km long, and has no along-channel bottom slope to minimize bottom bathymetry effects. The long estuarine channel is used to allow the salt intrusion to be fully developed under weak tides. The cross-channel section has a rectangular shape with a depth of 10 m and a width of 600 m. Freshwater discharge is specified at the head of the estuary, and a semidiurnal tide (S_2) is imposed at the eastern (seaward) boundary. The inflowing river water is prescribed to have zero salinity and a temperature of 15°C, identical to the background temperature set throughout the entire domain. The continental shelf is 80 km wide and has a fixed cross-shelf slope of 0.05%. The salinity of the coastal ocean is 35 practical salinity units (psu). A two-equation turbulence closure, $k-\omega$, is used to calculate vertical mixing [*Warner et al*., 2005].

[8] The model grid is 240 (along-channel, x direction) by 80 (cross-channel, y direction) by 20 (vertical, z direction) cells. The river has 200 grid cells along the channel and three grid cells across the channel. The small number of cross-channel cells is designed to minimize effects of lateral processes. The along-channel grid size (Δx) increases exponentially from the estuary's mouth ($\sim$100 m) to its head ($\sim$12 km), providing a highly resolved region

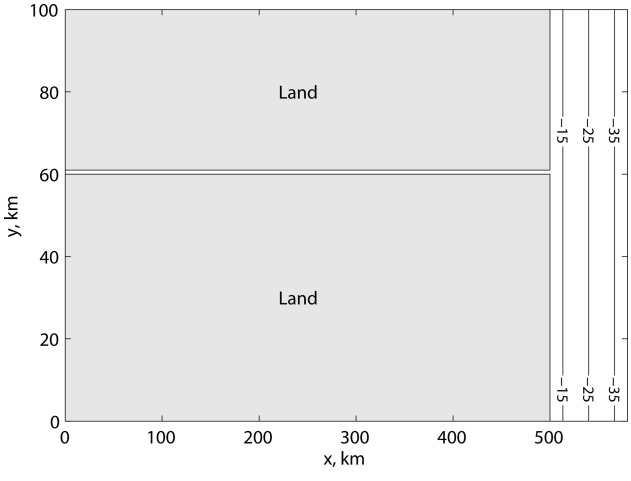

Figure 1. A schematic of the numerical model domain and bathymetry.

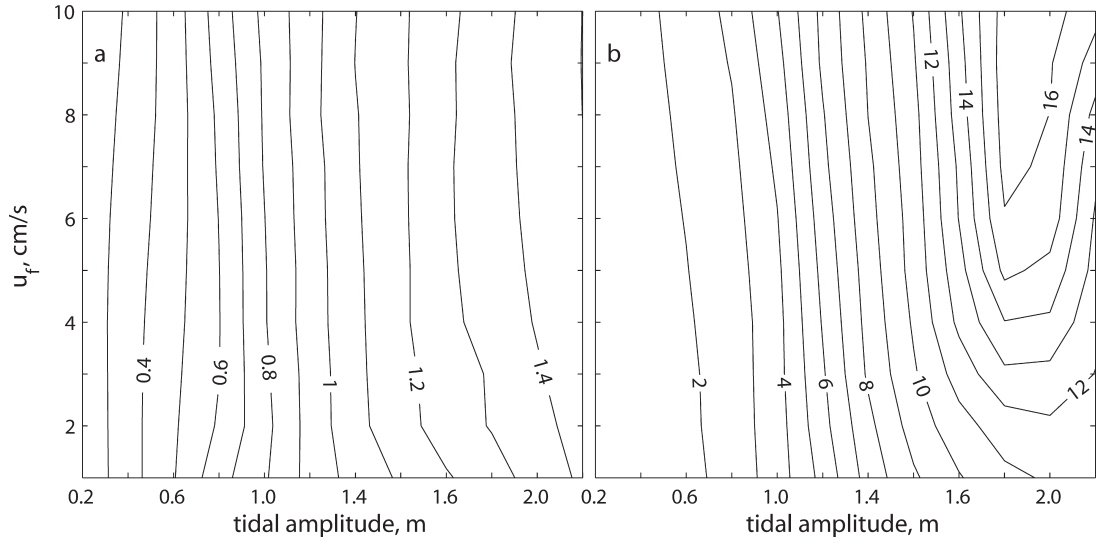

Figure 2. Major estuarine parameters shown as a function of tidal amplitude (m) at the ocean open boundary and the freshwater speed (cm s^{-1}) at the head of the estuarine channel. (a) Tidal current amplitude (m s^{-1}) at the mouth of estuaries and (b) longitudinal salinity gradient in the middle of estuaries (in units of $\times 10^{-4}$ psu m^{-1}).

near the mouth. The cross-channel grid and vertical layers are uniformly distributed. The model runs, from rest, for 4 months until reaching steady state. The results of the last day of simulation are used for analysis. Stratification in the estuary is determined by the competition between river discharge that provides buoyancy and tides that generate mixing. Various river discharge and tidal amplitude values were applied to generate different stratification conditions in the estuary (Figure 2). The section-averaged freshwater velocity was set from 1 to 10 cm s^{-1} (equivalent to discharges from 60 to 600 m^3 s^{-1}) at intervals of 1 cm s^{-1}, and tidal amplitudes ranged from 0.2 to 2.4 m at intervals of 0.2 m. The total number of numerical experiments performed was 120. Major estuarine parameters are shown in Figure 2 and the corresponding estuarine types are listed in Table 1.

Table 1. Estuarine Type of the Experiments[a]

	A											
u_f	0.2	0.4	0.6	0.8	1.0	1.2	1.4	1.6	1.8	2.0	2.2	2.4
1	−2	−2	−2	3	3	3	3	2	2	2	2	2
2	−2	−2	−2	3	3	3	3	3	3	2	2	2
3	−2	−2	−2	3	3	3	3	3	3	2	2	2
4	−2	−2	−2	3	3	3	3	3	3	2	2	2
5	−2	−2	−2	3	3	3	3	3	3	2	2	2
6	−2	−2	−2	3	3	3	3	3	3	2	2	2
7	−2	−2	−2	3	3	3	3	3	3	2	2	2
8	−2	−2	−2	3	3	3	3	3	3	2	2	2
9	−2	−2	−2	3	3	3	3	3	3	2	2	2
10	−2	−2	−2	3	3	3	3	3	3	2	2	2

[a]The numbers 2, 3, and −2 represent periodically stratified estuary that has a two-layer vertical structure of ATM-induced flow, weakly stratified estuary that has a three-layer vertical structure of ATM-induced flow in the central regime, and highly stratified estuary that has a reverse two-layer structure of ATM-induced flow, respectively. The unit for the freshwater velocity, u_f, is cm s^{-1}, and for the tidal amplitude, *A*, at the eastern open boundary is meters.

2.2. Decomposition of Residual Currents

[9] The decomposition of residual estuarine currents in an along-estuary section has been considered in several studies [e.g., *Burchard and Hetland*, 2010; *Burchard et al*., 2011; *Cheng et al*., 2011]. The decomposition method here is an improved version of that developed by *Cheng et al*. [2011] which used vertical *z* coordinates. First, a sigma coordinate transformation (nondimensional vertical coordinates) has been used for the momentum and continuity equations. This has been done in order to overcome the difficulty of calculating tidally averaged quantities in a surface layer that is influenced by tidal fluctuations of water level. Second, a complete decomposition of the along-estuary residual currents is provided with six contributions.

[10] The width-averaged governing equations for along-estuary momentum and continuity in sigma coordinates are given by

$$\frac{\partial u}{\partial t}+u\frac{\partial u}{\partial x}+\omega\frac{\partial u}{\partial \sigma}=-g\frac{\partial \eta}{\partial x}-\frac{g}{\rho_0}\left[\frac{\partial}{\partial x}\left(D\int_{\sigma}^{0}\rho \mathrm{d}\sigma'\right)+\rho\sigma\frac{\partial D}{\partial x}\right]+\frac{1}{D}\frac{\partial}{\partial \sigma}\left(\frac{K_m}{D}\frac{\partial u}{\partial \sigma}\right), \tag{1a}$$

$$\frac{\partial \eta}{\partial t}+\frac{\partial}{\partial x}\left(\int_{-1}^{0}Du\mathrm{d}\sigma\right)=0. \tag{1b}$$

[11] Here, $\sigma=(z-\eta)/D$, $D=\eta+H$, η is surface water elevation, H is the undisturbed water depth, u, w, ω ($\omega=\frac{D\sigma}{Dt}$) are velocity components in the along-estuary (x), vertical (z), and nondimensional vertical (σ) directions, respectively. When vertical sigma space is not uniform, D should be replaced with $\partial z/\partial\sigma$. Furthermore, t is time, K_m

is vertical eddy viscosity, g is gravity acceleration, ρ is water density, and ρ_0 is a reference density. Taking the time average of momentum and continuity over a tidal cycle gives

$$\overline{u\frac{\partial u}{\partial x}}+\overline{\omega\frac{\partial u}{\partial \sigma}}=-g\frac{\partial \overline{\eta}}{\partial x}-\frac{g}{\rho_0}\left[\frac{\partial}{\partial x}\left(\overline{D\int_{\sigma}^{0}\rho \mathrm{d}\sigma'}\right)+\overline{\rho\sigma\frac{\partial D}{\partial x}}\right]+\overline{Z}\frac{\partial}{\partial \sigma}\left(\overline{K_m}\frac{\partial \overline{u}}{\partial \sigma}\right)+\overline{Z}\frac{\partial}{\partial \sigma}\left(\overline{K'_m\frac{\partial u'}{\partial \sigma}}\right)+\overline{Z'\frac{\partial}{\partial \sigma}\left(\overline{K_m}\frac{\partial u'}{\partial \sigma}\right)}+\overline{Z'\frac{\partial}{\partial \sigma}\left(K'_m\frac{\partial \overline{u}}{\partial \sigma}\right)}+\overline{Z'\frac{\partial}{\partial \sigma}\left(K'_m\frac{\partial u'}{\partial \sigma}\right)}, \tag{2a}$$

$$(H+\overline{\eta})\int_{-1}^{0}\overline{u}\mathrm{d}\sigma+\int_{-1}^{0}\overline{\eta' u'}\mathrm{d}\sigma=R, \tag{2b}$$

where $u=\overline{u}+u'$, $\eta=\overline{\eta}+\eta'$, and R is the river discharge per unit of width. The overbar represents tidal average, a single prime indicates a time-varying quantity with zero mean. Similarly, K_m has been decomposed into $K_m=\overline{K_m}+K'_m$, and $1/D^2=\overline{Z}+Z'$. Note that using Taylor expansion, the first-order approximation of $1/D^2$ can be written as $1/D^2=1/H^2-2\eta/H^3$. However, calculating $\overline{Z}$ and Z' directly is not complicated. The tidal variation component of the vertical shear stress divergence has four components (the last four terms on the right-hand side of equation (2a), representing the covariance between eddy viscosity and vertical shear, the covariance between water level and shear, the covariance between water level and eddy viscosity, and the third-order correlation between water level, eddy viscosity, and vertical shear, respectively). In the absence of water surface fluctuations, the last three terms will drop out (those containing Z'). The sum of the four components is regarded as the driving force of asymmetric-tidal-mixing induced flow. On the left-hand side of the conservation of mass expression (equation (2b)), the first term represents the mean transport related to the mean flow and the second term represents Semi-Stokes transport (both evaluated in σ coordinates). Appendix A explains mean flow in terms of σ coordinates.

[12] The residual currents ($\overline{u}$) are considered to have six components: (1) the river-induced flow ($\overline{u_R}$); (2) the density-driven flow ($\overline{u_D}$); (3) the advection-induced flow ($\overline{u_A}$); (4) the flow induced by ATM ($\overline{u_T}$); (5) the Semi-Stokes return flow ($\overline{u_S}$), similar to Stokes drift compensation flow [*Jay*, 1991]; and (6) the wind-driven flow ($\overline{u_W}$). Thus, $\overline{u}$ and the corresponding residual water surface elevation, $\overline{\eta}$, can be written as

$$\overline{u}=\overline{u_R}+\overline{u_D}+\overline{u_A}+\overline{u_T}+\overline{u_S}+\overline{u_W}, \tag{3a}$$

$$\overline{\eta}=\overline{\eta_R}+\overline{\eta_D}+\overline{\eta_A}+\overline{\eta_T}+\overline{u_S}+\overline{\eta_W}. \tag{3b}$$

[13] Substituting equation (3) into equation (2) yields six groups of governing equations, each comprising a momentum and a continuity equation, corresponding to the six components of the residual currents. Details of the governing equations of the residual flows and their solutions are presented in Appendix B.

2.3. Estuarine Salt Transport

[14] Neglecting lateral processes and on subtidal time scales, the along-estuary advective salt flux in σ coordinates is written as

$$\overline{\int_{-1}^{0}Du(\sigma)s(\sigma)\mathrm{d}\sigma}=H\int_{-1}^{0}\overline{u}\overline{s}\mathrm{d}\sigma+\int_{-1}^{0}\overline{s}\overline{\eta u'}\mathrm{d}\sigma+H\int_{-1}^{0}\overline{u's'}\mathrm{d}\sigma+\int_{-1}^{0}\overline{u}\overline{\eta s'}\mathrm{d}\sigma+\int_{-1}^{0}\overline{\eta u's'}\mathrm{d}\sigma. \tag{4}$$

[15] Here, similar to the velocity, the salinity has been separated into tidal mean ($\overline{s}$) and tidal variation (s'):

$$s(\sigma)\approx\overline{s}+s'. \tag{5}$$

[16] The physical meaning of the terms on the right-hand side of equation (4) can be considered as follows: the first term represents salt transported by Eulerian residual currents, the second term represents Semi-Stokes transport of salt, and the remaining terms represent tidal pumping produced by (1) the tidal covariance of current and salinity, (2) the tidal covariance between water level and salinity, and (3) the third-order correlation of tidal variations in current, salinity, and water level. Because the contribution of tidal dispersion has not been generally quantified in estuaries, only the Eulerian residual transport of salt (first term on the right-hand side of equation (4)) is considered in this study. The residual current $\overline{u}$ can be obtained using the decomposition method (e.g., equation (3a)). In turn, the Eulerian mean transport of salt is decomposed into six contributions:

$$H\int_{-1}^{0}\overline{u}\overline{s}\mathrm{d}\sigma=H\int_{-1}^{0}(\overline{u_R}+\overline{u_D}+\overline{u_A}+\overline{u_T}+\overline{u_S}+\overline{u_W})\overline{s}\mathrm{d}\sigma. \tag{6}$$

3. Results

3.1. Vertical Distribution of ATM-Induced Flow

[17] Water column stratification is influential in the vertical distribution of ATM-induced flow. Three types of vertical patterns can be identified from the experiments corresponding to three types of estuaries, as represented by three selected experiments out of the 120 performed (Figure 3). Only the estuarine portion of the entire domain is shown to illustrate flow details. A periodically stratified estuary is an estuary in which stratification varies from well-mixed to stratified conditions during a tidal cycle. If an estuary is stratified during the entire tidal cycle, it can be further classified into weakly stratified and highly stratified. Unlike conventional classifications of estuaries, this classification is based on ATM and is different from that used in *Cheng et al*. [2011]. Details on this classification are given in section 4.3. In periodically stratified estuaries, which are equivalent to the weakly stratified estuaries in *Cheng et al*. [2011], the ATM-induced flow has a two-layer structure

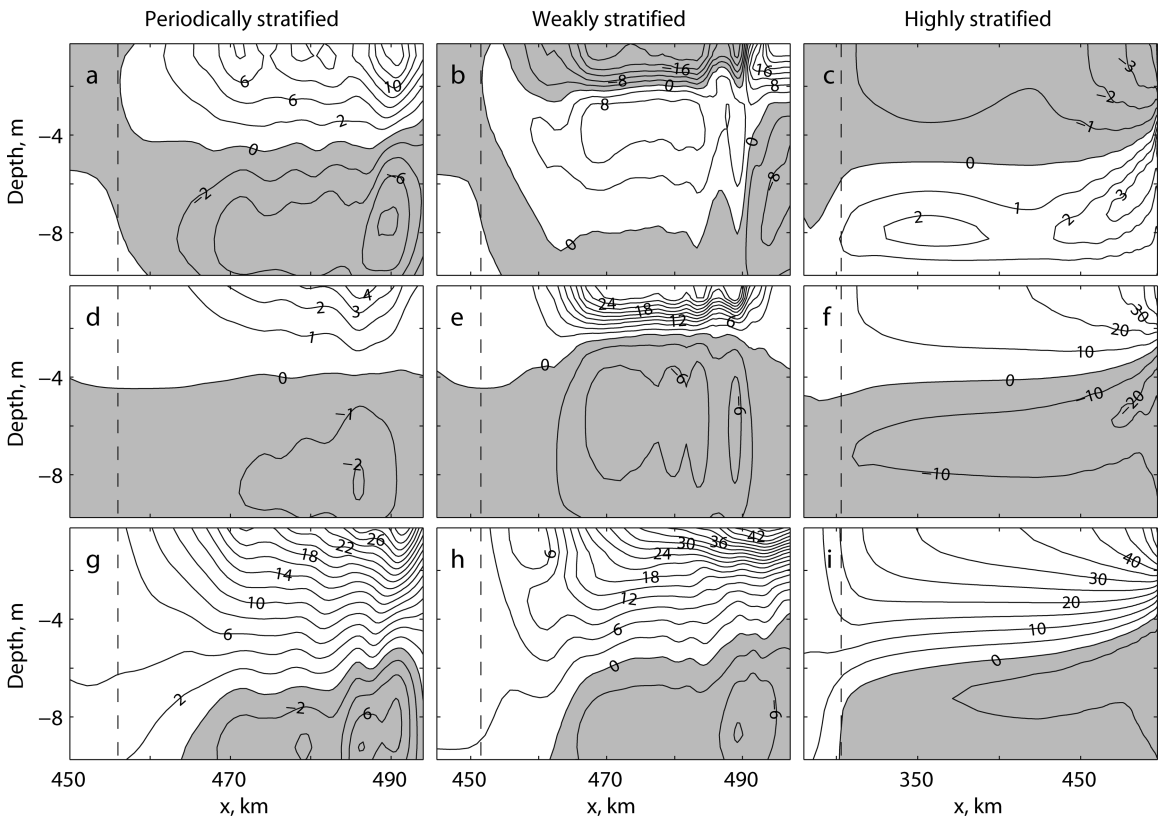

Figure 3. (top) Along-estuary distributions of the ATM-induced flow, (middle) the density-induced circulation, and (bottom) the total residual currents in the three types of estuaries. Negative values (shaded) represent landward currents. The mouth of the estuary is located at $x = 500$ km. The freshwater speed and the tidal amplitude at the open boundary are 1 cm s^{-1} and 1.8 m for the periodically stratified estuary, 2 cm s^{-1} and 1.2 m for the weakly stratified estuary, and 1 cm s^{-1} and 0.2 m for the highly stratified estuary. The vertical dashed lines show the upper limit of salt intrusion of each estuary.

with seaward flow near the surface and landward flow near the bottom. In weakly stratified estuaries, which include the partially mixed and highly stratified estuaries in *Cheng et al*. [2011], the ATM-induced flow has a three-layer structure in the central regime of the estuary with landward flow near the surface and the bottom, and seaward flow in the middle of the water column. In highly stratified estuaries, however, the residual flow generally exhibits a two-layer structure with landward flow near the surface and seaward flow near the bottom, opposing the density-driven flow. Previous studies have found that reversed ATM, i.e., stronger turbulent mixing during ebb than flood tides, can generate a residual flow opposite to the gravitational circulation [*Stacey et al*., 2008; *Cheng et al*., 2010]. In the numerical experiments of highly stratified estuaries performed here, turbulent mixing is consistently stronger during flood than ebb tides, indicating that other mechanisms produce the reverse two-layer residual flow.

[18] The vertical distribution of the ATM-induced flow is determined by the competition between two forcing mechanisms. This becomes evident by rewriting equation (B10a) as

$$\overline{u_\tau} = \int_{-1}^{\sigma} \frac{1}{\overline{\overline{K_m}}} \left(\frac{g}{\overline{\overline{Z}}} \frac{\partial \overline{\eta_T}}{\partial x} \sigma' - \overline{\left[K_m' \frac{\partial u'}{\partial \sigma} \right]} \right) d\sigma', \tag{7a}$$

$$\overline{\left[K_m' \frac{\partial u'}{\partial \sigma} \right]} = \overline{K_m'} \frac{\partial \overline{u'}}{\partial \sigma} - \frac{1}{\overline{\overline{Z}}} \left[\overline{Z' \frac{\partial}{\partial \sigma} \left(\overline{K}_m \frac{\partial u'}{\partial \sigma} \right)} + \overline{Z' \frac{\partial}{\partial \sigma} \left(K_m' \frac{\partial \overline{u}}{\partial \sigma} \right)} + \overline{Z' \frac{\partial}{\partial \sigma} \left(K_m' \frac{\partial u'}{\partial \sigma} \right)} \right], \tag{7b}$$

where the first component in the bracket of equation (7a) is the contribution that results from the residual water surface slope (or barotropic pressure gradient) and is referred to as the barotropic component. The second component in the bracket of equation (7a) follows from the second and third term of equation (B10a), and it involves the covariance between eddy viscosity and tidal shear and is referred to as a shear stress component. To compare their relative magnitudes, the two components without the minus sign of the second term are calculated in the middle of the three selected estuaries (Figure 4). Both components are negative (driving landward flows) and, as the shear stress component is preceded with a minus sign, it drives a seaward flow. The barotropic component is proportional with water depth and has a linear shape, while the vertical distribution of the shear stress component varies with different stratification conditions. In the periodically stratified estuary, the shear stress component tends to have a parabolic shape. It is larger than the barotropic component in the upper water

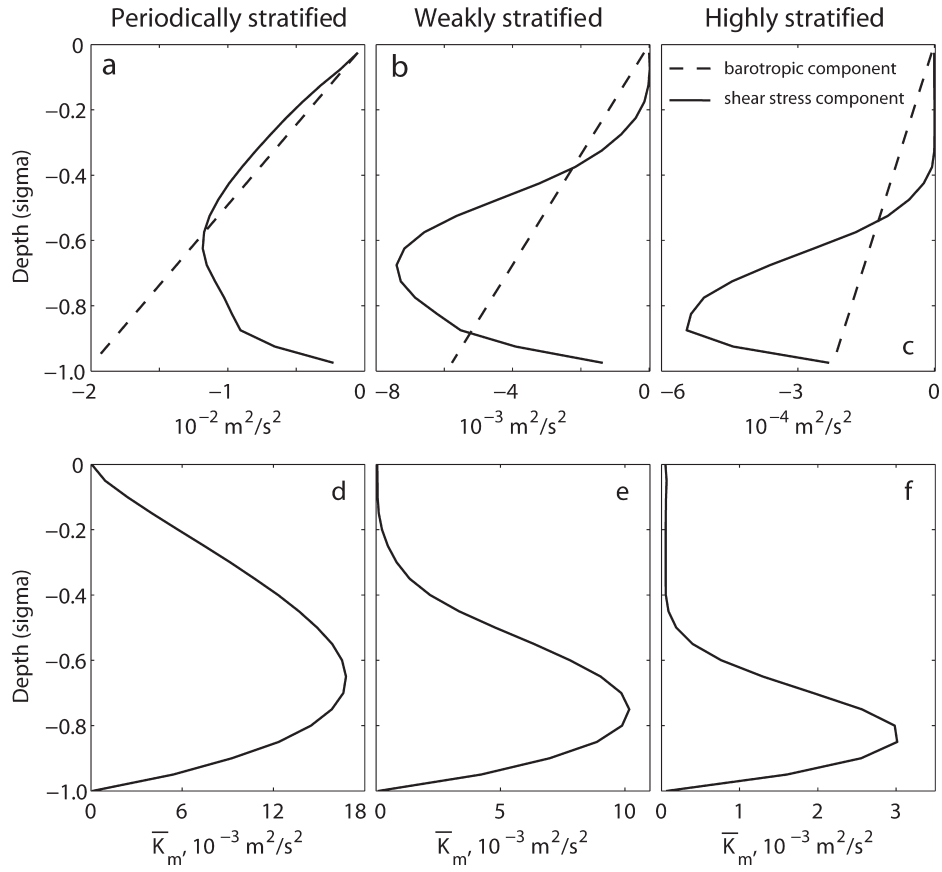

Figure 4. (top) Vertical distributions of the barotropic and shear stress components of the ATM-induced flow and (bottom) the tidally averaged eddy viscosity in the middle of the three types of estuaries, where the tidally averaged depth-mean salinity is half of that at the mouth (the selected experiments are the same as those shown in Figure 3). Negative stresses produce landward flow.

column and is smaller in the lower water column, resulting in a two-layer flow. With increased stratification, the shear stress component decreases in the upper water column and its maximum moves toward the bottom. Thus, in stratified estuaries the upper layer is dominated by a seaward flow. Note that the vertical distribution of the shear stress component is quite similar to that of the tidally averaged vertical eddy viscosity that shows that maximum viscosity is restricted to the lower water column. This indicates that the shear stress component and the vertical eddy viscosity are related, but this is a topic that will be explored in the future. In the weakly stratified estuary, the vertical patterns of the two forcing components in the lower water column are quite similar to those in the periodically stratified estuary, showing that ATM and its effects are restricted to the region below maximum viscosity (most turbulent flow). In the highly stratified estuary, the vertical patterns of the two forcing components in the lower water column are different from those in the weakly stratified estuary. As the seaward flow in the upper layer becomes dominant in the water column, the effect of ATM in producing residual currents might be altered in the lower water column.

3.2. Strength of ATM-Induced Flow

[19] As all components (except $\overline{u_R}$ and $\overline{u_S}$) of residual estuarine currents have zero vertical integral (see the continuity equation for residual currents in Appendix B), the intensity and the maximum vorticity are used to measure the strength of residual estuarine currents. The intensity of the ATM-induced flow, which is the depth-averaged magnitude (or absolute value) of residual flows, is computed in the middle of the simulated estuaries and plotted as a function of river flow velocity (u_f), i.e., the freshwater velocity specified at the head of the estuary channel, and of tidal current amplitude (U_T) at the estuary mouth (Figure 5a). The $u_f - U_T$ parameter space forms a prognostic classification of estuaries that predicts the estuarine regime based on the external forcing conditions [*Geyer*, 2010]. Although the numerical experiments cover a limited range of freshwater velocity and tidal current amplitude, the roles of river discharge and tide in the creation of ATM-induced flow can be inferred from the $u_f - U_T$ parameter space. In general, stronger tides produce relatively stronger ATM-induced flows and river flow has a relatively small effect, except for tidal currents larger than 0.8 m s^{-1}. The maximum strength of the ATM-induced flow appears in a region where the tidal current amplitude ranges from 1.0 to 1.2 m, and the freshwater velocity ranges from 7.0 to 9.0 cm s^{-1}, showing that the strength of the residual flow is not a monotonic function of river discharge or tidal current velocity. Some estuaries have been labeled in Figure 5a although this generic study has neglected lateral variability of bottom bathymetry, lateral advection, and Coriolis forcing that can contribute to the generation of internal tidal asymmetry in realistic estuaries. The purpose of Figure

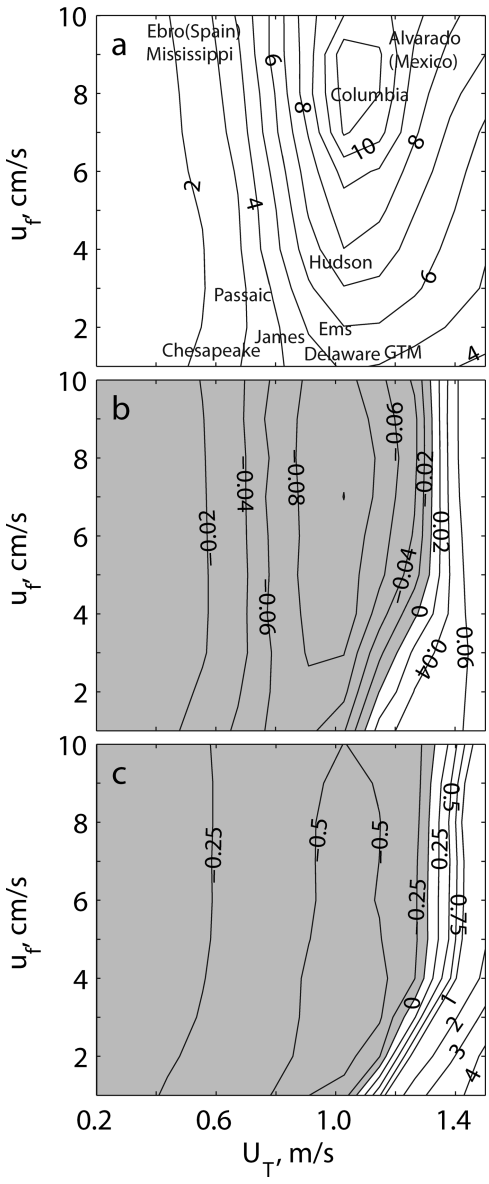

Figure 5. (a) Strength of ATM-induced flow in units of cm s^{-1}, (b) the maximum vorticity in units of s^{-1} of ATM-induced flow, and (c) the ratio between the maximum vorticity of ATM-induced and density-driven flows in the middle of estuaries, where the tidally averaged depth-mean salinity is half of that at the mouth, as a function of freshwater speed (u_f) and tidal current amplitude (U_T) at the estuary mouth. Marked estuaries are to show the relative importance of ATM-induced flow among these estuaries. GTM denotes Guana-Tolomato-Matanzas River in Florida. In Figure 5b, positive values indicate clockwise circulation and negative values indicate counterclockwise circulation; in (c) the ratios indicate that the ATM-induced flow either reinforces (positive values) or reduces (negative values) density-driven flow.

5a is to indicate the potential importance of ATM-induced flow in some estuaries.

[20] Because the magnitude of ATM-induced flows does not indicate the direction, and whether the ATM-induced flow reinforces or reduces the density-driven flow, the maximum vorticity ($\omega_y = \frac{\partial u}{\partial z} - \frac{\partial w}{\partial x} \approx \frac{\partial u}{\partial z}$) of both ATM-induced and density-driven flows was computed. Two extreme velocities were selected at the surface layer and the layers beneath to determine the velocity difference over the corresponding depth difference. The absolute values of the vorticity (up to 0.1 s^{-1}) are large, compared to planetary vorticity ($\sim 10^{-4}$ s^{-1}). In the coordinates of this study, the density-driven flow is always clockwise (positive values) while the ATM-induced flow could be either clockwise or counterclockwise (Figure 5b). The ratio between the maximum vorticity of the two residual flows indicates that the ATM-induced flow either reinforces (positive values) or reduces (negative values) the density-driven flow (Figure 5c). However, the ATM-induced flow does not compensate the density-driven flow (because the ratio is >-1) in any of the cases investigated in this study.

[21] Because stratification in estuaries is determined by the competition between river discharge and tides, the $u_f - U_T$ parameter space also indicates the influence of stratification on the strength of the ATM-induced flow. For a specific freshwater velocity, e.g., 8 cm s^{-1}, stratification decreases as the tidal current amplitude increases. The corresponding change in the strength of the ATM-induced flow is to increase (Figure 5a), reaching a maximum (at $\sim$1.1 m s^{-1}), and then to decrease. For a specific tidal current amplitude, e.g., 1.1 m s^{-1}, increasing freshwater velocity causes stratification enhancements, and the strength of the ATM-induced flow increases to a maximum and then decreases. The general relationship between the strength of ATM-induced flow and stratification, therefore, can be summarized as follows: the ATM-induced flow is strong in estuaries with moderate stratification and is weak in estuaries with weak and strong stratification. This relationship is expected from the shear stress component in the solution of the ATM-induced flow (equation (B10)), which is proportional to the tidal variation of shear stress and is inversely related to the tidally averaged vertical eddy viscosity. Strong tides may not only produce large tidal fluctuations of shear stress but also accompanying large vertical eddy viscosities. The reconciliation of the two parts results in the strongest ATM-induced flow in weakly stratified estuaries.

3.3. Relative Importance of ATM-Induced Flow

[22] The density-driven flow is conventionally considered the major component of residual estuarine currents. The relative importance of ATM in the creation of residual estuarine currents can be evaluated using the ratio between the strength of ATM-induced flow and of density-driven flow (Figure 6). In estuaries with strong tides ($U_T > 1$ to 1.2 m s^{-1}), the ratio is generally larger than 1.0, indicating that ATM is more important than the along-estuary density gradient in creating residual currents. The largest ratio occurs in the estuaries with the strongest tide and the lowest river discharge. In estuaries with moderate tidal currents, the ATM-induced flow has the same order of magnitude as the density-driven flow. In microtidal estuaries, the strength of the ATM-induced flow is $<50\%$ of the density-driven flow. In general, the ATM-induced flow dominates residual currents in periodically stratified estuaries and tends to be negligible in highly stratified estuaries.

[23] Low river discharges tend to favor the relative importance of ATM-induced flow, particularly with strong tides. Low river discharge allows increased turbulent mixing as well as salt intrusion length that leads to reduced

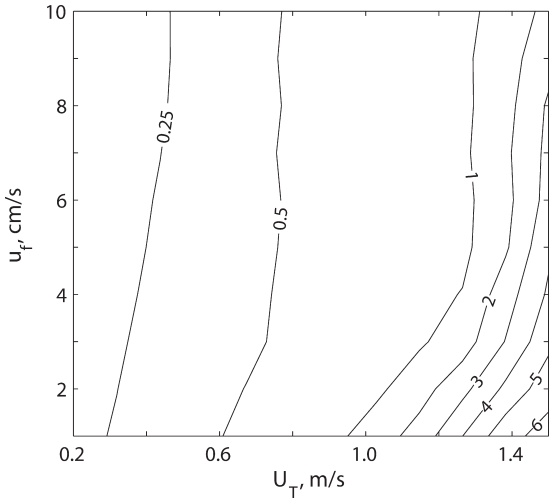

Figure 6. Ratio of the strength between ATM-induced flow and gravitational circulation in the middle of estuaries, where the tidally averaged depth-mean salinity is half of that at the mouth, as a function of freshwater speed (u_f) and tidal current amplitude (U_T) at the estuary mouth.

along-estuary density gradient. The strength of density-driven flow is related to both turbulent mixing and along-estuary gradient (e.g., equation (B8)). Therefore, the density-driven flow is more sensitive to river discharge than ATM-induced flow. Under low river discharge conditions, the decrease in density-driven flow turns out to be larger than that in ATM-induced flow, as a consequence, increasing the relative importance of ATM-induced flow.

3.4. Contribution of ATM-Induced Flow to Stratification

[24] The stratification of an estuary is determined by various mechanisms, among which residual currents could be an important contributor even at tidal time scales [*Simpson et al*., 1990]. In order to diagnose competing physical mechanisms of stratification and mixing, *Simpson et al*. [1990] developed a method based on a scalar parameter—potential energy anomaly (ϕ, in units of J m^{-3}) that is the work required to completely mix a unit water column. Following the potential energy anomaly approach, the contribution to the subtidal evolution of stratification from a residual flow, which has zero vertical integral, can be expressed as

$$\frac{\partial \phi}{\partial t} = \phi_t = g \frac{\partial \overline{[\rho]}}{\partial x} \int_{-1}^{0} \overline{u} z \sigma' \mathrm{d}\sigma, \tag{8}$$

where σ' is a dummy variable and the square brackets represent depth average. With the residual currents over one tidal cycle, the time rate of change of ϕ is calculated as one number that represents enhanced (positive values) or reduced (negative values) tidally averaged stratification. The potential energy anomaly equation contains other terms resulting from the expansion of density conservation (e.g., *Burchard and Hofmeister*, 2008; *de Boer et al*., 2008). However, those terms are neglected here as the focus is on the effect of the residual flow on stratification.

[25] Values of ϕ_t resulting from the ATM-induced and density-driven flows in the middle of estuaries are shown in the $u_f - U_T$ parameter space (Figure 7). As expected, the density-driven flow tends to enhance stratification in all estuaries. In comparison, the ATM-induced flow tends to enhance stratification in estuaries with strong tides and weak river discharge, and to reduce stratification in estuaries with weak tides and strong river discharge. The contribution of flow to stratification depends on the vertical structure of the flow. Given a typical density field that increases toward the bottom, the ATM-induced flow with a two-layer structure similar to that of the density-driven

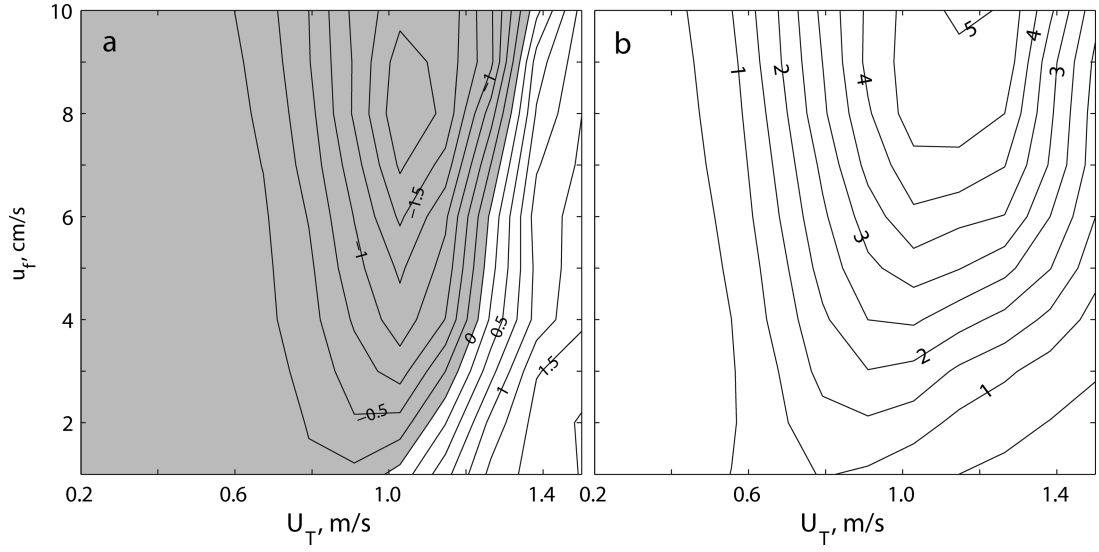

Figure 7. Contributions of (a) ATM-induced flow and (b) density-driven flow to tidally averaged stratification represented with potential energy anomalies (the contours are in units of J m^{-3} s^{-1}) in the middle of estuaries, where the tidally averaged depth-mean salinity is half of that at the mouth, as a function of freshwater speed (u_f) and tidal current amplitude (U_T) at the estuary mouth. Positive values denote increasing stratification.

flow tends to increase stratification, while that with a reverse two-layer structure tends to decrease stratification. The ATM-induced flow with a three-layer structure could either increase or decrease stratification. Comparing the magnitudes of ϕ_t resulting from the two types of residual flows, the contribution to stratification from the density-driven flow is generally larger than that from the ATM-induced flow although the latter could be stronger in periodically stratified estuaries (largest tidal forcing and smallest river discharge in Figure 7).

3.5. Contribution of ATM-Induced Flow to Subtidal Salt Transport

[26] ATM influences salt transport through both mean flow and tidal dispersion. In view of harmonic analysis, the asymmetric tidal current velocity during a tidal cycle results from the combined effect of tide and overtide contributions [*Jay*, 1991]. The overtide alters the phase relationship between tidal currents and salinity. As a consequence, it also modifies the salt flux transported by tidal dispersion. Thus, ATM can contribute to net mass transport, particularly sediment transport [*Jay* and Musiak, 1994]. However, it is still difficult to quantify the contribution of ATM to tidal dispersion of salt and the role of tidal dispersion in estuarine salt balance. Here, the focus is only on salt transport caused by ATM-induced flow and on its comparison to density-driven flow, such that the relative importance of ATM-induced flow in estuarine salt balance (e.g., equation (6)) can be evaluated.

[27] Figure 8 shows the ratio of net salt flux transported by ATM-induced and density-driven flows (e.g., $\int_{-1}^{0} \overline{u_T s}\mathrm{d}\sigma / \int_{-1}^{0} \overline{u_D s}\mathrm{d}\sigma$) in the middle of the estuaries within the $u_f - U_T$ parameter space. Density-driven flow consistently drives salt landward, while ATM-induced flow exhibits different behaviors because of its relatively complicated vertical patterns. In estuaries with strong tides ($U_T > 1.1$ m s^{-1}), ATM-induced flow transports salt in the same direction as density-driven flow, and produces larger net salt transports under small river discharge conditions. In estuaries with weak tides, ATM-induced flow transports salt in the opposite direction to density-driven flow, and generally produces small salt transports. In weakly stratified estuaries, ATM-induced flow transports negligible salt because of the three-layer vertical pattern. The comparison of the contributions of ATM-induced and density-driven flows to salt transport indicates that ATM-induced flow is an important mechanism that can drive down-gradient salt transport in many estuaries. Not including ATM-induced flow in an estuarine salt balance will cause underestimates of salt intrusion length in systems with strong tides and overestimates in estuaries with weak tides.

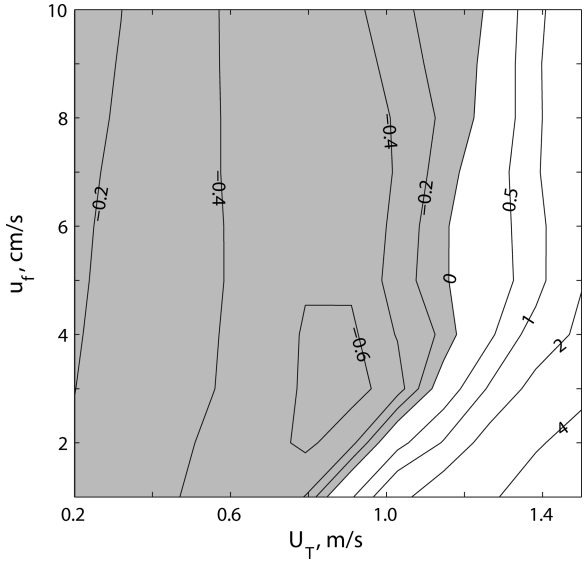

Figure 8. Ratio of salt transport due to ATM-induced flow and due to density-driven flow in the middle of estuaries, where the tidally averaged depth-mean salinity is half of that at the mouth, as a function of freshwater speed (u_f) and tidal current amplitude (U_T) at the estuary mouth. Positive values denote that the two salt fluxes have the same direction.

4. Discussion

4.1. Driving Mechanisms of ATM

[28] Tidal variations of stratification can be generated by a variety of mechanisms such as tidal straining [*Simpson et al*., 1990], freshwater sources from side embayments of the estuary [*Lacy et al*., 2003; *Fram et al*., 2007], and lateral advection terms [*Burchard and Schuttelaars*, 2012]. Due to the simplified numerical model configuration that excluded side freshwater sources and minimized lateral processes, asymmetries in stratification were mainly driven by tidal straining which can be evaluated using the temporal variations in potential energy anomaly, ϕ:

$$\frac{\partial \phi}{\partial t} = g\frac{\partial \overline{[\rho]}}{\partial x}\int_{-1}^{0} \overline{u}\sigma' \mathrm{d}\sigma = g\frac{\partial \overline{[\rho]}}{\partial x}\int_{-1}^{0} \left(\hat{u}' + \bar{\hat{u}}\right)\sigma' \mathrm{d}\sigma, \qquad (9)$$

where $\hat{u} = u - [u]$ is the anomaly from the depth-mean flow and was further separated into tidal variation ($\hat{u}'$) and tidal mean ($\bar{\hat{u}}$). The first part of the straining term represents tidal straining and the second part is due to straining of density by mean flow (hereafter called residual straining). A detailed examination of vertical eddy viscosities, potential energy anomalies, and tidal and residual straining in the middle of the three selected experiments is shown in Figure 9. In all three estuaries, turbulent mixing is stronger during flood than ebb tides (Figures 9a–9c), but the tidal variations of stratification and straining are different.

[29] In the periodically stratified estuary, stratification (Figure 9d) is weaker during flood than ebb, in accordance with turbulent mixing. Tidal straining reduces stratification during flood (negative values) and enhances stratification during ebb (positive values). In contrast, residual straining tends to enhance stratification but it is negligible compared to the strength of tidal straining (Figure 9g). The consistency of mixing, stratification, and tidal straining indicates that tidal straining is responsible for the ATM and is the driving force for ATM-induced flow.

[30] In the weakly stratified estuary, stratification is stronger in flood than in ebb, showing a tidal cycle of stratification (Figure 9e) opposite to that indicated by the vertical eddy viscosities. However, this is not surprising. The

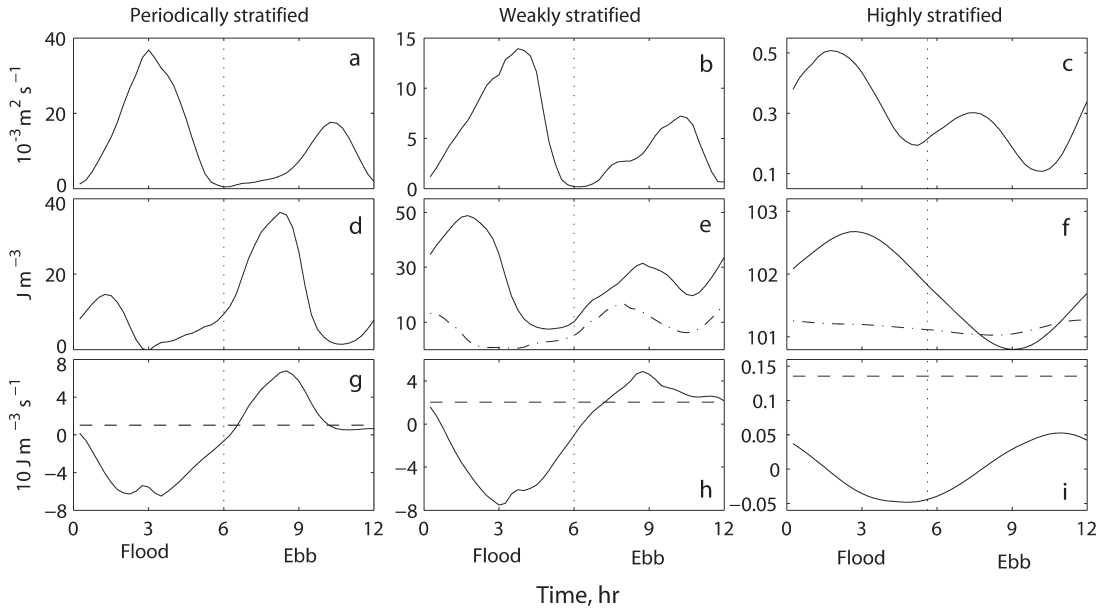

Figure 9. (a–c) Tidal evolution of the depth-mean eddy viscosity, (d–f) potential energy anomaly, (solid lines, g–i) tidal straining, and (dashed lines, g–i) residual straining in the middle of the three types of estuaries, where the tidally averaged depth-mean salinity is half of that at the mouth. The vertical dot lines show the transition between flood and ebb tides. The dot-dashed line in Figures 9e and 9f shows the potential energy anomaly within the bottom boundary layer.

stratification of a water column is determined by both tidal mixing and background stratification. For a stratified water column, tides mix the bottom boundary layer of which the height is set by the interaction of turbulence with the overlying stratification [*Stacey and Ralston*, 2005], but increase the stratification of the entire water column. Stronger tidal mixing during the flood would result in more pronounced stratification than during the ebb. Excluding the top stratified layer, the potential energy anomaly of the bottom boundary layer that extends from the bottom to 2.5 m below the surface exhibits similar temporal evolution (the dot-dashed line in Figure 9e) to that in the periodically stratified estuary. Tidal straining generally reduces stratification during the flood and enhances stratification during the ebb, controlling the evolution of stratification within the bottom boundary layer. Residual straining becomes relatively more important, but its magnitude remains much smaller than that of tidal straining in this case (Figure 9h). For this type of estuaries, the bottom boundary layer is an analogous to the periodically stratified estuaries.

[31] In the highly stratified estuary, stratification is stronger during flood than ebb tides (Figure 9f). The potential energy anomaly of the bottom boundary layer shows similar evolution to that of the entire water column (the dot-dashed line in Figure 9f) so that the bottom boundary layer is different from the periodically stratified estuary. Tidal straining still generally reduces stratification during flood and increases stratification during ebb. However, residual straining exceeds tidal straining (Figure 9i), indicating that the residual flow dominates over tidal currents. To better understand tidal evolution of the shear flow, hourly vertical profiles of the along-estuary current during a tidal cycle in the middle of the highly stratified estuary is shown in Figure 10. It is evident that the thickness of the bottom boundary layer, which is determined using maximum vertical salinity gradient (it can also be seen visually from the velocity profiles) varies intratidally. However, it does not extend closer than 5 m from the water surface such that a seaward flow

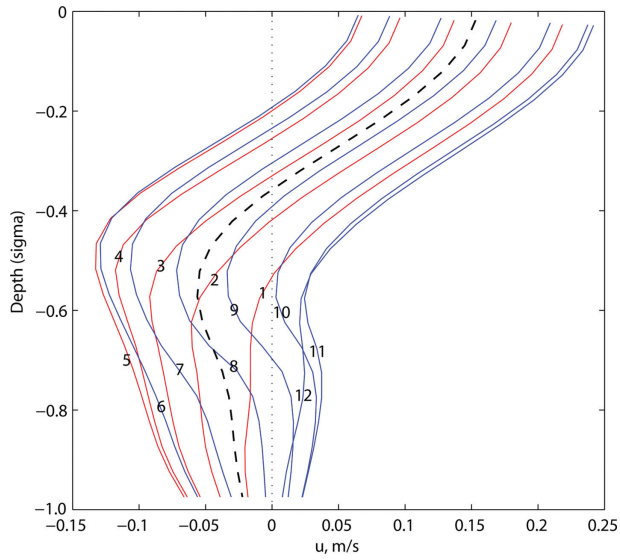

Figure 10. Hourly profiles of the along-estuary current velocity in the middle of the highly stratified estuary, where the tidally averaged depth-mean salinity is half of that at the mouth, over a tidal cycle. The dashed line shows the tidally averaged velocity, while the dotted line represents the zero line. Negative values denote landward currents. Time (in hours, is labeled on the curves) starts from the beginning of flood as indicated by the depth-averaged tidal current velocity.

persistently dominates the top layer. The bottom boundary layer seems to be embedded in a background two-layer (or residual) circulation with seaward flow near the surface and landward flow near the bottom. The flood currents flow into the estuary near the bottom, increasing stratification of the entire water column and becoming more sheared than in other tidal phase, even though tidal mixing is relatively strong (Figure 9c). During ebb, stratification decreases and the tidal currents in the bottom boundary layer are less sheared than during flood. The bottom landward background flow prolongs the duration and reinforces the strength of flood flows, generating a tidal asymmetry in the bottom boundary layer that causes a landward residual flow (Figure 3c). The unique characteristics of the tidal bottom boundary layer in the highly stratified estuary result from the existence of a background two-layer circulation that has the same order of magnitude as (even larger than) that of the tidal currents. Tidal currents are then regulated by the residual flow, which is mainly a combination of the density-driven and river-induced flows (e.g., gravitational circulation).

[32] The tidal mixing process in narrow estuaries is related to the thickness of the bottom boundary layer. If the bottom boundary layer extends to the surface, as in periodically stratified estuaries, tidal straining determines the tidal evolution of stratification of the entire water column. If the bottom boundary layer is restricted to the lower water column, as in stratified estuaries, tidal straining only determines the tidal evolution of stratification within the bottom boundary layer. In particular, if the bottom boundary layer is confined to near bottom, as in highly stratified estuaries, the residual flow alters tidal currents and causes tidal asymmetries in vertical shear that are different from the tidal-straining-induced tidal asymmetry. The tidal mixing processes in periodically and weakly stratified estuaries are consistent with the observations in the Columbia River [*Jay*, 1991], while the residual-flow-induced tidal asymmetry in highly stratified estuaries occurs when tides are weak.

[33] The height of the bottom boundary layer (h_{BBL}) relative to the water depth in a stratified water column is given by *Stacey and Ralston* [2005]:

$$\frac{h_{\mathrm{BBL}}}{H} = \left(\frac{R_{\mathrm{fc}}}{Ri_x}\right)^{1/2}, \tag{10a}$$

$$Ri_x = \frac{\frac{g}{\rho_0}\frac{\partial \bar{\rho}}{\partial x} H^2}{C_d U_T^2}, \tag{10b}$$

where R_{fc} is the critical flux Richardson number and is chosen as 0.2, Ri_x is the horizontal Richardson number (or referred to as the Simpson number, *Burchard and Hetland*, 2010), and C_d is the bottom drag coefficient (with a typical value of 0.0025). The nondimensional bottom boundary layer height clearly separates the numerical experiment results in three groups corresponding to the three types of estuaries (Table 2). An estuary is periodically stratified when the relative height of the bottom boundary layer is larger than nearly 0.85, and becomes highly stratified when the thickness of the bottom boundary layer is less than 0.65 the water depth. Although the critical values of the limits separating the three types of estuaries inferred from the numerical experiments might not be universal, the bottom boundary layer thickness (as in equation (10a)) can indeed be used to measure estuarine stratification.

[34] Internal tidal asymmetry implies that tidal currents do not reverse throughout the water column during a tidal period in which ebb currents are more vertically sheared than flood currents. This asymmetry is related to the varying stratification caused by tidal straining [*Jay*, 1991]. As stratification is often linked to turbulent mixing, internal tidal asymmetry was described as the imbalance of magnitude of eddy viscosity between flood and ebb tides (e.g., ATM) [*Cheng et al*., 2010, 2011]. However, in highly stratified estuaries, the tidal asymmetry in tidal velocity profile within the bottom boundary layer is regulated by the residual flow rather than by tidal straining. To account for various mechanisms producing tidal variations of the tidal velocity profile, a broader definition of internal tidal asymmetry is suggested to replace ATM in future work. In this definition, internal tidal asymmetry simply represents the asymmetries in the vertical shear of tidal currents during a tidal cycle, regardless of the causes of tidal asymmetries in the current velocity profile. Thus, the tidal covariance of eddy viscosity and vertical shear can act as the force of internal tidal asymmetry in the tidally averaged momentum equation.

4.2. Scaling of ATM-Induced Flow

[35] As tidal straining was considered the dominant driving mechanism for ATM, the strength of ATM-induced

Table 2. Nondimensional Height of Bottom Boundary Layer in the Middle of the Estuaries[a]

	A											
u_f	0.2	0.4	0.6	0.8	1.0	1.2	1.4	1.6	1.8	2.0	2.2	2.4
1	0.26	0.37	0.54	0.68	0.76	0.77	0.81	0.84	0.87	0.90	0.93	0.95
2	0.25	0.38	0.54	0.69	0.74	0.77	0.79	0.82	0.84	0.89	0.93	0.95
3	0.26	0.39	0.56	0.70	0.75	0.76	0.78	0.79	0.83	0.87	0.91	0.94
4	0.27	0.40	0.58	0.71	0.75	0.76	0.78	0.80	0.82	0.87	0.87	0.92
5	0.27	0.42	0.59	0.72	0.75	0.76	0.78	0.79	0.82	0.86	0.85	0.90
6	0.28	0.43	0.60	0.72	0.75	0.76	0.78	0.79	0.81	0.84	0.84	0.89
7	0.28	0.44	0.61	0.72	0.74	0.76	0.78	0.79	0.81	0.86	0.85	0.90
8	0.29	0.44	0.62	0.72	0.74	0.76	0.78	0.79	0.81	0.85	0.85	0.91
9	0.29	0.45	0.62	0.72	0.74	0.76	0.77	0.79	0.80	0.85	0.86	0.91
10	0.31	0.45	0.62	0.71	0.73	0.75	0.77	0.78	0.80	0.84	0.86	0.90

[a]The middle of the estuary is defined as the location where the tidally averaged depth-mean salinity is half that at the mouth. The unit for the freshwater velocity, u_f, is cm s^{-1}, and for the tidal amplitude, A, at the eastern open boundary is meters.

flow has been scaled using the horizontal Richardson number that measures the competition between tidal straining and tidal stirring to determine stratification in an estuary [*Simpson et al.*, 1990; *Monismith et al.*, 1996; *Stacey et al.*, 2001]. Numerical results (not shown) display a linear relationship between Ri_x and the strength of ATM-induced flow for periodically stratified estuaries, similar to the finding of *Burchard and Hetland* [2010], but no clear relationship in the weakly and highly stratified estuaries. In the definition of the horizontal Richardson number (e.g., equation (10a)), the friction velocity u_* is approximated using the bottom drag (e.g., $u_*^2 = C_d U_T^2$). This is appropriate for well-mixed estuaries but does not account for the effect of stratification on bottom shear stress. With the numerical model, the friction velocity can be directly calculated and was used to replace $C_d U_T^2$ in equation (10b) with a scale of the friction velocity, U_*^2, which is the mean of squared friction velocity over a tidal cycle. The strength of ATM-induced flows is now found to be, in general, linearly related to the updated Ri_x (Figure 11a). The correlation coefficient (r^2) is highest for periodically stratified estuaries (0.92) and is also significant for weakly stratified estuaries (0.87). This confirms that tidal straining is the main driving force for ATM in those two types of estuaries. However, a general relationship is not found for highly stratified estuaries, where results are separated into three groups corresponding to different tidal forcing. Because tidal asymmetries in the vertical shear of tidal currents are determined by the residual flow in this type of estuaries, Ri_x is not the appropriate indicator of ATM-induced flow, so further studies are needed.

[36] The analytical study of *Cheng et al.* [2010] has shown that the strength of ATM-induced flow is proportional to the imbalance of turbulent mixing between flood and ebb tides in periodically stratified estuaries. Here, a nondimensionial parameter K_a is proposed to measure the asymmetries in tidal mixing:

$$K_a = \frac{\int_0^T -\mathrm{sign}([u])[K_m]\mathrm{d}t}{\int_0^T [K_m]\mathrm{d}t}, \tag{11}$$

where T is the tidal period. The depth-averaged flow velocity, $[u]$, is assumed positive during flood, and negative during ebb. The sign of $[u]$ is given to $[K_m]$ to compute "net" turbulent mixing. The physical meaning of K_a is the normalized excess of turbulent mixing over a tidal cycle. The parameter has a range from -1 to 1, with larger absolute values representing stronger asymmetries in tidal mixing. Positive K_a indicates typical ATM (more mixing during flood than ebb), while negative K_a indicates reverse ATM (more mixing in ebb than flood). A zero value of K_a represents symmetric tidal mixing. The results in periodically stratified estuaries support a clear linear relation between the strength of ATM-induced flow and K_a (Figure 11b). Moreover, the linear relation also exists in weakly stratified estuaries as asymmetric shear of tidal currents in this type of estuaries can be generally represented by tidal mixing (e.g., stronger sheared flow relates to weak mixing within the bottom boundary layer). In highly stratified estuaries, the strength of ATM-induced flow is insensitive to K_a because of different driving mechanisms of ATM.

4.3. Classification of Estuaries in a View of Tidal Variation of Stratification

[37] Coastal plain estuaries are conventionally classified into three types: well mixed, partially stratified, and highly stratified on the basis of their stratification and salinity characteristics [*Cameron and Pritchard*, 1963]. Quantitative schemes developed to classify and compare estuaries, such as the Hansen-Rattray diagram [*Hansen and Rattray*, 1966], mainly rely on estimates of tidally averaged salinity

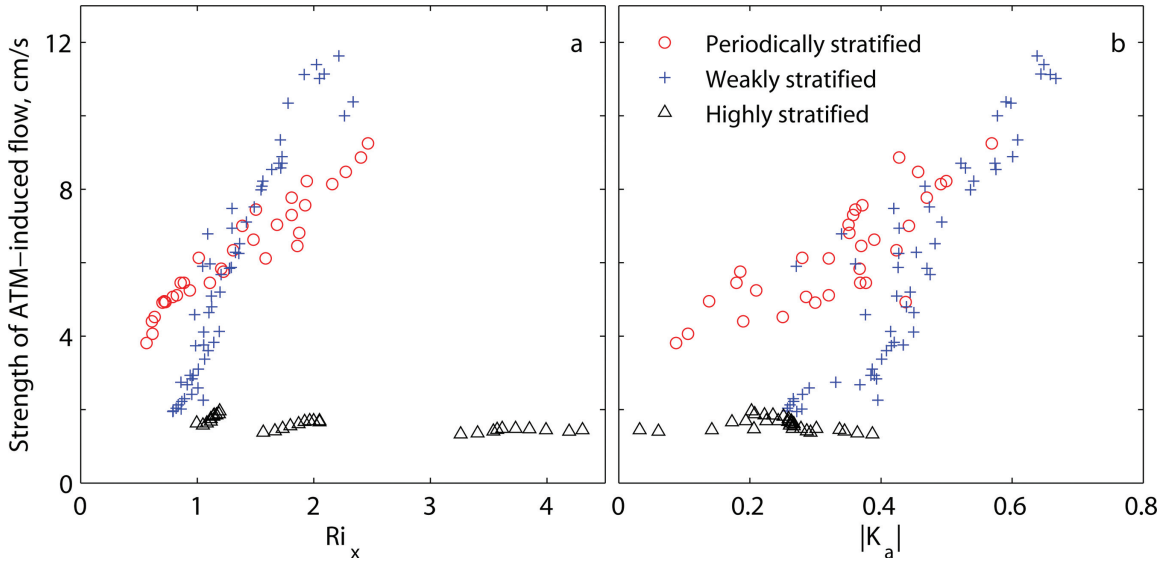

Figure 11. (a) Strength of ATM-induced flow as a function of the horizontal Richardson number and (b) the magnitude of asymmetries in tidal mixing represented with K_a in the middle of estuaries, where the tidally averaged depth-mean salinity is half of that at the mouth. The three types of estuaries are represented with different symbols.

and gravitational circulation. Despite the success of those classification schemes, *Dyer* [1997] pointed out that "the main restriction is that the classification is for tidally averaged conditions, and gives no information concerning the processes that are related to the effects of a finite amplitude tide, or the variations within the tide." Here, a classification of estuaries is proposed from a different point of view, i.e., the tidal variation of stratification. The purpose is not to develop a new classification system, but rather to emphasize the importance of tidal processes in subtidal estuarine dynamics.

[38] The temporal evolution of stratification in a narrow estuary can be described using the equation of stratification obtained by vertically differentiating the salt conservation equation [*Nepf and Geyer*, 1996]:

$$\frac{\partial}{\partial t}\frac{\partial s}{\partial \sigma}+\frac{\partial \overline{u}}{\partial \sigma}\frac{\partial s}{\partial x}+\frac{\partial u'}{\partial \sigma}\frac{\partial s}{\partial x}=\frac{1}{D^2}\frac{\partial^2}{\partial \sigma^2}\left(K_s\frac{\partial s}{\partial z}\right), \tag{12}$$

where K_s is the vertical eddy diffusivity of salt. The along-estuary current velocity u has been decomposed into a tidal mean ($\overline{u}$) plus a tidal fluctuation component (u'). Thus, the second term on the left-hand side of the equation represents residual straining coming from the contribution of residual currents and the third term represents tidal straining. The term on the right-hand side of the equation represents tidal stirring [*Simpson et al*., 1990]. Residual straining increases stratification and tidal stirring reduces stratification. Tidal straining reduces stratification during flood tides and increases it during ebb tides. Such competition between straining and stirring ultimately determines the stratification of the estuary during a tidal cycle.

[39] Two extreme cases are considered. First, if the estuary is well mixed during ebb tides when tidal stirring is larger than tidal straining plus residual straining that might be negligible, the estuary must be well mixed over the entire tidal period. This is a well-mixed estuary. Second, if the estuary is stratified during flood tides when residual straining is larger than tidal stirring plus tidal straining, the estuary must be stratified over the entire tidal period. This is a stratified estuary. The estuary between the two extremes is periodically stratified. Stratified estuaries can be further separated into weakly stratified and highly stratified. The criterion to identify the two types is not straightforward. As discussed in the previous section, the estuary becomes highly stratified when residual straining dominates stratification or the contribution of tidal straining to stratification is negligible. In contrast to the density-driven flow that always has a two-layer structure, the ATM-induced flow exhibits distinct characteristics in different types of estuaries. A summary of the classification of estuaries is proposed in Table 3. This classification is similar to the conventional classification of coastal plain estuaries but emphasizes the importance of both residual and tidal currents. The class of weakly stratified estuary might contain some estuaries that have strong tides and belong to a highly stratified estuary in the conventional classification.

[40] To quantify stratification, the tidally averaged horizontal Richardson number (e.g., equation (10b) with the mean of squared friction velocity over a tidal period) and the top to bottom salinity difference in the middle of the estuaries are shown in the $u_f - U_T$ space (Figure 12). It has been suggested that tidal straining leads to periodic stratification if the tidally averaged Ri_x exceeds ~0.2 [*Li et al*., 2008]. The tidally averaged horizontal Richardson numbers of the experiments are generally larger than 0.2, consistent with the fact that none of the simulated estuaries is well-mixed. Compared to top to bottom salinity difference, Ri_x is not monotonically related to stratification. In periodically stratified estuaries, Ri_x is linearly related to top to bottom salinity difference because tidal staining dominates the tidal evolution of stratification and stronger tides lead to weaker stratification. In weakly stratified estuaries, Ri_x is generally inversely related to top to bottom salinity difference. This is because tidal straining contributes to tidal evolution of stratification in an opposite way to that in periodically stratified estuaries so that stronger tides lead to stronger stratification. In highly stratified estuaries, Ri_x generally shows a similar trend as the top to bottom salinity difference because residual straining determines stratification, and weak tides occur with strong residual currents that lead to stronger stratification.

Table 3. Classification of Estuaries Based on Tidal Mixing

	ATM-Induced Flow	
Category	Vertical Structure	Relative Importance
Well mixed	None	None
Periodically stratified	Two layer	Dominant
Weakly stratified	Three layer	As important as density-driven flow
Highly stratified	Reverse two layer	Negligible

[41] As shown in previous studies [*Simpson et al*., 1990; *Monismith et al*., 1996; *Stacey et al*., 2001], Ri_x is a convenient parameter to distinguish a well-mixed estuary from a stratified estuary. This is because tidal straining and tidal stirring are the dominant processes controlling stratification in periodically stratified estuaries. In weakly and highly stratified estuaries, residual straining becomes important. Moreover, advection of horizontal density gradients and lateral straining, which Ri_x does not account for, have been found to make relevant contributions to determine stratification in realistic estuaries [*Stacey et al*., 2008; *Giddings et al*., 2011; *Scully and Geyer*, 2012]. Hence, the relationship between Ri_x and stratification is rather complicated in stratified estuaries with realistic bathymetry.

5. Summary and Conclusions

[42] This study examines the characteristics of ATM-induced flow in different types of estuaries. In the tidally averaged momentum equation, ATM is represented as the covariance of eddy viscosity and vertical shear. The covariance is found to drive a seaward flow while the corresponding residual water surface slope drives a landward flow. The competition between the two components determines the vertical distribution of the ATM-induced flow. The barotropic component is proportional to water depth showing a linear vertical profile, while the shear stress component is influenced by stratification. As a result, the ATM-induced flow has a two-layer vertical structure in periodically stratified estuaries, a three-layer vertical structure in the central regime of weakly stratified estuaries, and a reverse

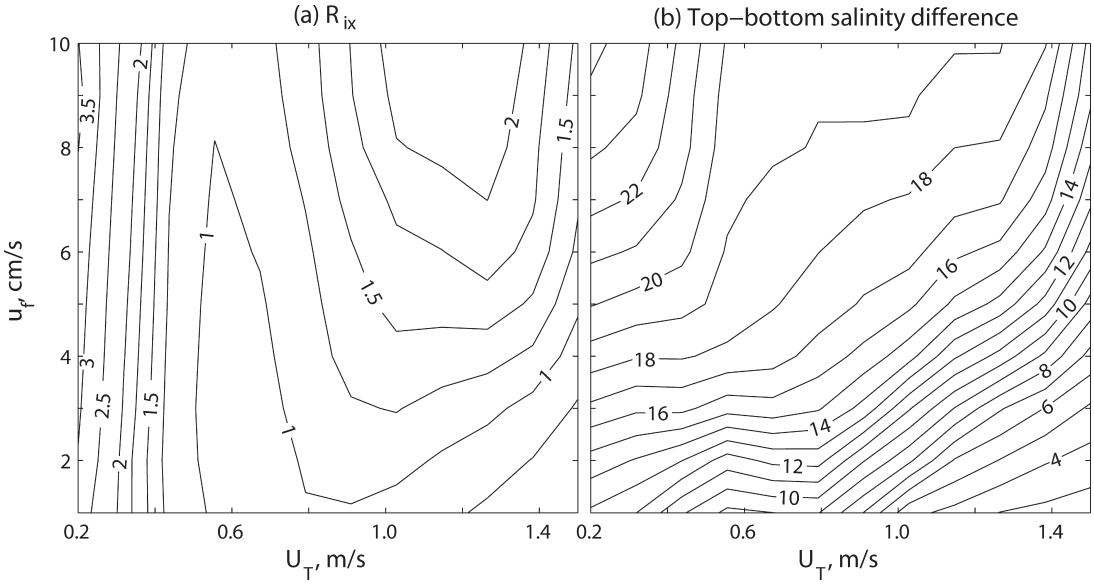

Figure 12. (a) Horizontal Richardson number and (b) top-to-bottom salinity difference in the middle of estuaries, where the tidally averaged depth-mean salinity is half of that at the mouth, as a function of freshwater speed (u_f) and tidal current amplitude (U_T) at the estuary mouth.

two-layer structure in highly stratified estuaries. As a consequence of the different vertical distributions, the ATM-induced flow contributes to either reinforce or reduce tidally averaged stratification, and transport salt in the same direction or in the opposite direction to the density-driven flow.

[43] The driving mechanisms of ATM are related to the thickness of the bottom boundary layer relative to the water depth. The bottom boundary layer occupies nearly the entire water column in periodically stratified estuaries, and most of the lower water column of weakly stratified estuaries. Tidal straining controls the tidal variations of velocity profile in the bottom boundary layer of the two types of estuaries, and the magnitude of ATM-induced flow is approximately proportional to the horizontal Richardson number and to ATM (K_a). In highly stratified estuaries with weak tides, where the bottom boundary layer is restricted near the bottom, ATM is related to the background residual flow that regulates tidal currents and is negligible in creating residual flow compared to the longitudinal density gradient.

[44] Conventional theory of estuarine dynamics has focused mainly on gravitational circulation as the responsible for stratification and salt transport in estuaries. This study, however, has shown that ATM-induced flow is also an essential component of estuarine circulation and particularly plays a crucial role in stratification and salt balance in periodically stratified estuaries. Furthermore, the decomposition method suggests that estuarine circulation has multiple components resulting from a variety of mechanisms. This fact indicates that the discrepancies between observations and the conventional theory found in many estuaries might come from the effects of the other components of estuarine circulation. To fully understand subtidal estuarine dynamics, in-depth examination of ATM-induced flow as well as other residual flows in realistic estuarine environments is needed in future studies.

Appendix A: Mean Flow and Stokes Transport in σ Coordinates

[45] The relationship between along-channel velocity u in σ coordinates and along-channel velocity $\tilde{u}$ in z coordinates reads

$$u(x,\sigma,t) = \tilde{u}(x,z(\sigma),t), \tag{A1a}$$

$$z(\sigma) = \sigma H + (1+\sigma)\eta. \tag{A1b}$$

[46] An explicit, approximate, relationship between mean flow $\overline{u}$, evaluated at a fixed level and mean flow $\tilde{u}$, evaluated at a fixed position can be derived by writing $z = \overline{z} + z'$, where $\overline{z}$ is the mean height of the surface σ (=constant) and $z' = (1+\sigma)\eta'$ its tidal fluctuating part. Now, by assuming that sea surface variations are small compared to mean depth, it follows that (where "$< >$" denotes a time average, applied at a fixed z)

$$\overline{u}\ (x,\sigma) \simeq\ \tilde{u}(x,\ \bar{z}) + (1+\sigma) < \eta'\frac{\partial \tilde{u}}{\partial z}|_{z=\bar{z}} >. \tag{A2}$$

[47] This result shows that $\overline{u}$, the time mean velocity in σ coordinates, is a semi-Lagrangian mean velocity, in the sense that it is evaluated at a level $\sigma =$ constant that, from an Eulerian perspective, varies in time. The term semi-Lagrangian, rather than Lagrangian, is used to stress that no individual particles are followed, but only the movement of the σ surface. Likewise, the second term on the right-hand side of equation (A2) can be interpreted as a semi-Stokes velocity.

[48] Finally, the mean flow component $\overline{u}_S$ (in σ coordinates) is considered. According to equation (A2), this component is forced by the mean transport

$$\overline{q}_s \equiv \int_{-1}^{0} \overline{\eta' u'}\,\mathrm{d}\sigma = \eta'\left(\int_{-1}^{0} u\ \mathrm{d}\sigma\right)', \tag{A3}$$

which is defined here as the Stokes transport in σ coordinates. It results from covariance between the tidal fluctuating parts of the sea surface and of the depth-averaged velocity. This variable is not identical to the Stokes transport $<q_S>$ in z coordinates, defined as

$$\langle q_S \rangle \equiv \langle \int_{\overline{\eta}}^{\eta} \tilde{u}'\, dz \rangle. \tag{A4}$$

[49] Clearly, $<q_S>$ results from covariance between the sea surface fluctuations and the depth-averaged fluctuating part of the velocity between mean sea level and the actual sea level. As the latter velocity is larger than or equal to the full-depth-averaged velocity, it follows that the Stokes transport in σ coordinates, ($\overline{q}_S$ in A3), is smaller than or equal to the Stokes transport $<q_S>$ in z coordinates. The equal sign holds when the velocity is independent of the vertical coordinate.

Appendix B: Decomposition of Along-Estuary Residual Currents

[50] The governing equations for each component include:

$$0 = -g\frac{\partial \overline{\eta_R}}{\partial x} + \overline{Z}\frac{\partial}{\partial \sigma}\left(\overline{K_m}\frac{\partial \overline{u_R}}{\partial \sigma}\right), \tag{B1a}$$

$$\int_{-1}^{0} H\overline{u_R}\,\mathrm{d}\sigma = R, \tag{B1b}$$

for river-induced flow,

$$0 = -g\frac{\partial \overline{\eta_D}}{\partial x} - \frac{g}{\rho_0}\left[\frac{\partial}{\partial x}\left(\overline{D\int_{\sigma}^{0}\rho \mathrm{d}\sigma'}\right) + \overline{\rho\sigma\frac{\partial D}{\partial x}}\right] + \overline{Z}\frac{\partial}{\partial \sigma}\left(\overline{K_m}\frac{\partial \overline{u_D}}{\partial \sigma}\right), \tag{B2a}$$

$$\int_{-1}^{0} H\overline{u_D}\,\mathrm{d}\sigma = 0, \tag{B2b}$$

for density-driven flow,

$$\overline{u\frac{\partial u}{\partial x}} + \omega\frac{\partial \overline{u}}{\partial \sigma} = -g\frac{\partial \overline{\eta_A}}{\partial x} + \overline{Z}\frac{\partial}{\partial \sigma}\left(\overline{K_m}\frac{\partial \overline{u_A}}{\partial \sigma}\right), \tag{B3a}$$

$$\int_{-1}^{0} H\overline{u_A}\,\mathrm{d}\sigma = 0, \tag{B3b}$$

for advection-induced flow,

$$0 = -g\frac{\partial \overline{\eta_T}}{\partial x} + \overline{Z}\frac{\partial}{\partial \sigma}\left(\overline{K_m}\frac{\partial \overline{u_T}}{\partial \sigma}\right) + \overline{Z}\frac{\partial}{\partial \sigma}\left(\overline{K'_m\frac{\partial u'}{\partial \sigma}}\right) + \overline{Z'\frac{\partial}{\partial \sigma}\left(\overline{K_m}\frac{\partial u'}{\partial \sigma}\right)} + \overline{Z'\frac{\partial}{\partial \sigma}\left(K'_m\frac{\partial \overline{u}}{\partial \sigma}\right)} + \overline{Z'\frac{\partial}{\partial \sigma}\left(K'_m\frac{\partial u'}{\partial \sigma}\right)}, \tag{B4a}$$

$$\int_{-1}^{0} H\overline{u_T}\,\mathrm{d}\sigma = 0, \tag{B4b}$$

for ATM-induced flow,

$$0 = -g\frac{\partial \overline{\eta_S}}{\partial x} + \overline{Z}\frac{\partial}{\partial \sigma}\left(\overline{K_m}\frac{\partial \overline{u_S}}{\partial \sigma}\right), \tag{B5a}$$

$$\int_{-1}^{0} H\overline{u_S}\,\mathrm{d}\sigma + \int_{-1}^{0} \overline{\eta u'}\,\mathrm{d}\sigma = 0, \tag{B5b}$$

for Stokes return flow, and

$$0 = -g\frac{\partial \overline{\eta_W}}{\partial x} + \overline{Z}\frac{\partial}{\partial \sigma}\left(\overline{K_m}\frac{\partial \overline{u_W}}{\partial \sigma}\right), \tag{B6a}$$

$$\int_{-1}^{0} H\overline{u_W}\,\mathrm{d}\sigma = 0, \tag{B6b}$$

for wind-driven flow. The boundary conditions used to solve the governing equations for each residual flow are no shear at the surface and no slip at the bottom, except the wind-driven flow for which the surface shear stress is equal to wind stress (i.e., τ_W). To calculate wind-driven flow, the wind must be steady. The solution for river-induced flow is

$$\overline{u_R} = \frac{g}{\overline{Z}}\frac{\partial \overline{\eta_R}}{\partial x}\int_{-1}^{\sigma}\frac{\sigma'}{\overline{K_m}}\mathrm{d}\sigma', \tag{B7a}$$

$$\frac{\partial \overline{\eta_R}}{\partial x} = \frac{\overline{Z}R}{gH\int_{-1}^{0}\int_{-1}^{\sigma}\frac{\sigma'}{\overline{K_m}}\mathrm{d}\sigma'\mathrm{d}\sigma}. \tag{B7b}$$

[51] The solution for density-driven flow is

$$\overline{u_D} = \frac{g}{\overline{Z}}\frac{\partial \overline{\eta_D}}{\partial x}\int_{-1}^{\sigma}\frac{\sigma'}{\overline{K_m}}\mathrm{d}\sigma' - \frac{g}{\overline{Z}\rho_0}\int_{-1}^{\sigma}\left\{\frac{1}{\overline{K_m}}\int_{\sigma'}^{0}\left[\int_{\sigma''}^{0}\frac{\partial \overline{D\rho}}{\partial x}\mathrm{d}\sigma''' + \overline{\rho\sigma''}\frac{\partial D}{\partial x}\right]\mathrm{d}\sigma''\right\}\mathrm{d}\sigma', \tag{B8a}$$

$$\frac{\partial \overline{\eta_D}}{\partial x} = \frac{\int_{-1}^{0}\int_{-1}^{\sigma}\left\{\frac{1}{\overline{K_m}}\int_{\sigma'}^{0}\left[\int_{\sigma''}^{0}\frac{\partial \overline{D\rho}}{\partial x}\mathrm{d}\sigma''' + \overline{\rho\sigma'''}\frac{\partial D}{\partial x}\right]\mathrm{d}\sigma''\right\}\mathrm{d}\sigma'\mathrm{d}\sigma}{\rho_0\int_{-1}^{0}\int_{-1}^{\sigma}\frac{\sigma'}{\overline{K_m}}\mathrm{d}\sigma'\mathrm{d}\sigma}. \tag{B8b}$$

[52] The solution for advection-induced flow is

$$\overline{u_A} = \frac{g}{\overline{Z}}\frac{\partial \overline{\eta_A}}{\partial x}\int_{-1}^{\sigma}\frac{\sigma'}{\overline{K_m}}\mathrm{d}\sigma' - \frac{1}{\overline{Z}}\int_{-1}^{\sigma}\left[\frac{1}{K_m}\int_{\sigma'}^{0}\left(\overline{u\frac{\partial u}{\partial x}} + \overline{\omega\frac{\partial u}{\partial \sigma''}}\right)\mathrm{d}\sigma''\right]\mathrm{d}\sigma', \tag{B9a}$$

$$\frac{\partial \overline{\eta_A}}{\partial x} = \frac{\int_{-1}^{0}\int_{-1}^{\sigma}\left[\frac{1}{\overline{K_m}}\int_{\sigma'}^{0}\left(\overline{u\frac{\partial u}{\partial x}} + \overline{\omega\frac{\partial u}{\partial \sigma''}}\right)\mathrm{d}\sigma''\right]\mathrm{d}\sigma'\mathrm{d}\sigma}{g\int_{-1}^{0}\int_{-1}^{\sigma}\frac{\sigma'}{\overline{K_m}}\mathrm{d}\sigma'\mathrm{d}\sigma}. \tag{B9b}$$

[53] The solution for ATM-induced flow is

$$\overline{u_T} = \frac{g}{\overline{Z}}\frac{\partial \overline{\eta_T}}{\partial x}\int_{-1}^{\sigma}\frac{\sigma'}{\overline{K_m}}\mathrm{d}\sigma' - \int_{-1}^{\sigma}\frac{1}{\overline{K_m}}\overline{K'_m\frac{\partial u'}{\partial \sigma'}}\mathrm{d}\sigma' + \frac{1}{\overline{Z}}\int_{-1}^{\sigma}\left\{\frac{1}{K_m}\int_{\sigma'}^{0}\left[\overline{Z'\frac{\partial}{\partial \sigma''}\left(\jmath K_m{}^{\jmath}\frac{\partial u'}{\partial \sigma''}\right)} + \overline{Z'\frac{\partial}{\partial \sigma''}\left(K'_m\frac{\partial \overline{u}}{\partial \sigma''}\right)} + \overline{Z'\frac{\partial}{\partial \sigma''}\left(K'_m\frac{\partial u'}{\partial \sigma''}\right)}\right]\mathrm{d}\sigma''\right\}\mathrm{d}\sigma', \tag{B10a}$$

$$\frac{\partial \overline{\eta_T}}{\partial x} = \frac{\overline{Z}\displaystyle\int_{-1}^{0}\int_{-1}^{\sigma}\frac{1}{\overline{K_m}}\overline{K'_m\frac{\partial u'}{\partial \sigma'}}\mathrm{d}\sigma'\mathrm{d}\sigma}{g\displaystyle\int_{-1}^{0}\int_{-1}^{\sigma}\frac{\sigma'}{\overline{K_m}}\mathrm{d}\sigma'\mathrm{d}\sigma} - \frac{\displaystyle\int_{-1}^{0}\int_{-1}^{\sigma}\left\{\frac{1}{K_m}\int_{\sigma'}^{0}\left[\overline{Z'\frac{\partial}{\partial \sigma''}\left(\overline{K_m}\frac{\partial u'}{\partial \sigma''}\right)} + \overline{Z'\frac{\partial}{\partial \sigma''}\left(K'_m\frac{\partial \overline{u}}{\partial \sigma''}\right)} + \overline{Z'\frac{\partial}{\partial \sigma''}\left(K'_m\frac{\partial u'}{\partial \sigma''}\right)}\right]\mathrm{d}\sigma''\right\}\mathrm{d}\sigma'\mathrm{d}\sigma}{g\displaystyle\int_{-1}^{0}\int_{-1}^{\sigma}\frac{\sigma'}{\overline{K_m}}\mathrm{d}\sigma'\mathrm{d}\sigma}. \tag{B10b}$$

[54] The solution for Stokes return flow is

$$\overline{u_S} = \frac{g}{\overline{Z}}\frac{\partial \overline{\eta_S}}{\partial x}\int_{-1}^{\sigma}\frac{\sigma'}{\overline{K_m}}\mathrm{d}\sigma', \tag{B11a}$$

$$\frac{\partial \overline{\eta_S}}{\partial x} = \frac{-\overline{Z}\displaystyle\int_{-1}^{0}\overline{\eta u'}d\sigma}{gH\displaystyle\int_{-1}^{0}\int_{-1}^{\sigma}\frac{\sigma'}{\overline{K_m}}\mathrm{d}\sigma'\mathrm{d}\sigma}. \tag{B11b}$$

[55] Finally, the solution for wind-driven flow is

$$\overline{u_W} = \frac{g}{\overline{Z}}\frac{\partial \overline{\eta_W}}{\partial x}\int_{-1}^{\sigma}\frac{\sigma'}{K_m}\mathrm{d}\sigma' + \tau_W\int_{-1}^{\sigma}\frac{1}{\overline{K_m}}\mathrm{d}\sigma', \tag{B12a}$$

$$\frac{\partial \overline{\eta_W}}{\partial x} = \frac{-\overline{Z}\tau_W\displaystyle\int_{-1}^{0}\int_{-1}^{\sigma}\frac{1}{\overline{K_m}}\mathrm{d}\sigma'\mathrm{d}\sigma}{g\displaystyle\int_{-1}^{0}\int_{-1}^{\sigma}\frac{\sigma'}{\overline{K_m}}\mathrm{d}\sigma'\mathrm{d}\sigma}. \tag{B12b}$$

[56] Here, σ' and $\sigma'\prime$ are dummy variables. In the continuity equations, $\overline{\eta}$ was excluded to simplify the formulae. Note that the solutions of $\overline{u_R}$, $\overline{u_D}$, $\overline{u_A}$, and $\overline{u_T}$ are considered the σ coordinates transformation of those under z coordinates in *Cheng et al*. [2011].

[57] **Acknowledgments.** P.C. acknowledges support from President Research Award of Xiamen University. Arnoldo Valle-Levinson acknowledges support from Utrecht University and the Fulbright Commission. The authors are grateful to the three anonymous reviewers for their insightful comments that greatly improved this work.

References

Burchard, H., and R. D. Hetland (2010), Quantifying the contributions of tidal straining and gravitational circulation to residual circulation in periodically stratified tidal estuaries, *J. Phys. Oceanogr.*, *40*, 1243–1262.

Burchard, H., and R. Hofmeister (2008), A dynamics equation for the potential energy anomaly for analyzing mixing and stratification in estuaries and coastal seas, *Estuarine Coastal Shelf Sci.*, *77*, 679–687.

Burchard, H., and H. Schuttelaars (2012), Analysis of tidal straining as driver for estuarine circulation in well mixed estuaries, *J. Phys. Oceanogr.*, *42*, 261–271.

Burchard, H., R. D. Hetland, E. Schulz, and H. M. Schuttelaars (2011), Drivers of residual estuarine circulation in tidally energetic estuaries: Straight and irrotational channels with parabolic cross section, *J. Phys. Oceanogr.*, *41*, 548–570.

Cameron, W. M., and D. W. Pritchard (1963), *Estuaries*, in *The Sea*, vol. *2*, edited by M. N. Hill, pp. 306–324, John Wiley, New York.

Chatwin, P. C. (1976), Some remarks on the maintenance of the salinity distribution in estuaries, *Estuarine Coastal Mar. Sci.*, *4*, 555–566.

Cheng, P., A. Valle-Levinson, and H. E. de Swart (2010), Residual currents induced by asymmetric tidal mixing in weakly stratified narrow estuaries, *J. Phys. Oceanogr.*, *40*, 2135–2147.

Cheng, P., A. Valle-Levinson, and H. E. de Swart (2011), A numerical study of residual circulation induced by asymmetric tidal mixing in tidally dominated estuaries, *J. Geophys. Res.*, *116*, C01017, doi:10.1029/2010JC006137.

de Boer, G. J., J. D. Pietrzak, and J. C. Winterwerp (2008), Using the potential energy anomaly equation to investigate tidal straining and advection of stratification in a region of freshwater influence, *Ocean Modell.*, *22*, 1–11.

Dyer, K. R. (1997), *Estuaries: A Physical Introduction*, 2nd ed., John Wiley, Chichester, U. K.

Fram, J. P., M. Martin, and M. T. Stacey (2007), Exchange between the coastal ocean and a semi-enclosed estuarine basin: Dispersive fluxes, *J. Phys. Oceanogr.*, *37*, 1645–1660.

Geyer, W. R. (2010), Estuarine salinity structure and circulation, in *Contemporary Issues in Estuarine Physics*, edited by A. Valle-Levinson, pp. 12–26, Cambridge Univ., Cambridge, U. K.

Geyer, W. R., J. H. Trowbridge, and M. M. Bowen (2000), The dynamics of a partially mixed estuary, *J. Phys. Oceanogr.*, *30*, 2035–2048.

Giddings, S. N., D. A. Fong, and S. G. Monismith (2011), Role of straining and advection in the intratidal evolution of stratification, vertical mixing, and longitudinal dispersion of a shallow, macrotidal, salt wedge estuary, *J. Geophys. Res.*, *116*, C03003, doi:10.1029/2010JC006482.

Haidvogel, D. B., H. G. Arango, K. Hedstrom, A. Beckmann, P. Malanotte-Rizzoli, and A. F. Shchepetkin (2000), Model evaluation experiments in the North Atlantic Basin: Simulations in nonlinear terrain-following coordinates, *Dyn. Atmos. Oceans*, *32*, 239–281.

Hansen, D. V., and M. Rattray (1965), Gravitational circulation in straits and estuaries, *J. Mar. Res.*, *23*, 104–122.

Hansen, D. V., and M. Rattray (1966), New dimensions in estuary classification, *Limnol. Oceanogr.*, *11*(3), 319–326.

Ianniello, J. P. (1977), Tidally induced residual currents in estuaries of breadth and depth, *J. Mar. Res.*, *35*, 755–786.

Jay, D. A. (1991), Internal asymmetry and an harmonicity in estuarine flows, in *Process in Tidal Hydrodynamics*, edited by B. B. Parker, pp. 521–546, John Wiley, New York.

Jay, D. A., and J. D. Musiak (1994), Particle trapping in estuarine tidal flows, *J. Geophys. Res.*, *99*, 445–461.

Lacy, J. R., M. T. Stacey, J. R. Burau, and S. G. Monismith (2003), The interaction of lateral baroclinic forcing and turbulence in an estuary, *J. Geophys. Res.*, *108*(C3), 3089, doi:10.1029/2002JC001392.

Li, C., and J. O'Donnell (2005), The effects of channel length on the residual circulation in tidally dominated channels, *J. Phys. Oceanogr.*, *35*(10), 1826–1840.

Li, M., J. Trowbridge, and W. R. Geyer (2008), Asymmetric tidal mixing due to the horizontal density gradient, *J. Phys. Oceanogr.*, *38*, 418–434.

Monismith, S. G., W. Kimmerer, J. R. Burau, and M. T. Stacey (2002), Structure and flow-induced variability of the subtidal salinity field in Northern San Francisco Bay, *J. Phys. Oceanogr.*, *32*, 3003–3019.

Nepf, H. M., and W. R. Geyer (1996), Intratidal variations in stratification and mixing in the Hudson estuary, *J. Geophys. Res.*, 101, 12079–12086.

Pritchard, D. W. (1956), The dynamic structure of a coastal plain estuary, *J. Mar. Res.*, *15*(1), 33–42.

Scully, M. E., and W. R. Geyer (2012), The role of advection, straining, and mixing on the tidal variability of estuarine stratification, *J. Phys. Oceanogr.*, *42*, 855–868.

Shchepetkin, A. F., and J. C. McWilliams (2005), The Regional Ocean Modeling System (ROMS): A split-explicit, free-surface, topography-following coordinates ocean model, *Ocean Modell.*, *9*, 347–404.

Simpson, J. H., J. Brown, J. Matthews, and G. Allen (1990), Tidal straining, density currents, and stirring in the control of estuarine stratification, *Estuaries*, *13*(2), 125–132.

Stacey, M. T., and D. K. Ralston (2005), The scaling and structure of the estuarine bottom boundary layer, *J. Phys. Oceanogr.*, *35*(1), 55–71.

Stacey, M. T., J. R. Burau, and S. G. Monismith (2001), Creation of residual flows in a partially stratified estuary, *J. Geophys. Res.*, *106*(8), 17,013–17,037.

Stacey, M. T., J. P. Fram, and F. K. Chow (2008), Role of tidally periodic density stratification in the creation of estuarine subtidal circulation, *J. Geophys. Res.*, *113*, C08016, doi:10.1029/2007JC004581.

Warner, J. C., C. R. Sherwood, H. G. Arango, and R. P. Signell (2005), Performance of four turbulence closure models implemented using a generic length scale method, *Ocean Modell.*, *8*, 81–113.

Winant, C. D. (2008), Three-dimensional residual tidal circulation in an elongated, rotating basin, *J. Phys. Oceanogr.*, *38*(6), 1278–1295.

Zimmerman, J. T. F. (1980), Vorticity transfer by tidal currents over an irregular topography, *J. Mar. Res.*, *38*(4), 601–630.